FEBS 18721 FEBS Letters 411 (1997) 19–26

The NMR solution structure of the NMDA receptor antagonist, conantokin-T, in the absence of divalent metal ions

Scott E. Warder[a], Zhigang Chen[b], Yi Zhu[b], Mary Prorok[a], Francis J. Castellino[a], Feng Ni[b,*]

[a]*Department of Chemistry and Biochemistry and the Center for Transgene Research, University of Notre Dame, Notre Dame, IN 46556, USA*
[b]*Biomolecular NMR Laboratory and the Montreal Joint Centre for Structural Biology, Biotechnology Research Institute, National Research Council of Canada, 6100 Royalmount Avenue, Montreal, Quebec H4P 2R2, Canada*

Received 18 February 1997; revised version received 22 April 1997

Abstract The solution conformation of conantokin-T, a Gla-containing 21-residue peptide, ($G_1E\gamma\gamma Y_5QKML\gamma_{10}NLR\gamma A_{15}$-EVKK$N_{20}$A-amide), in the absence of divalent metal ions, was studied by use of two-dimensional proton NMR spectroscopy. The peptide is helical from the N-terminus to the C-terminus, as defined by upfield-shifted α-proton resonances and by characteristic NOE connectivities. Extensive interactions among the amino acid side-chains were identified from the NOESY spectra of this peptide in a buffered aqueous solution. Four hydrophobic residues Tyr[5], Met[8], Leu[9], and Leu[12] contact one another in a stable cluster, even in the presence of 6 M urea. The solution structure of conantokin-T is a well-defined α-helix, having RMSD values for the backbone and all heavy atoms of 0.40 Å and 0.77 Å, respectively. Potential repulsion between the negatively-charged side chains of Gla[10] and Gla[14] is minimized by a Gln[6]-Gla[10] hydrogen bond and by an Arg[13]-Gla[14] ion-pair interaction. The C-terminal amide and the Asn[20] side-chain amide both interact with the backbone and minimize fraying at the C-terminal end of the α-helix. This study provides a basis to evaluate the changes in peptide conformation concomitant upon the binding of divalent metal ions. In addition, this investigation demonstrates that apo-conantokin-T has almost all of the favorable interactions that are known to contribute to helical stabilization in proteins and monomeric helices.

Key words: Conantokin-T; Peptide folding; NMDA receptor; Helical polypeptides; *gamma*-Carboxyglutamate

1. Introduction

The survival and proliferation of snails belonging to the genus *Conus* is due to the development of remarkable peptide warfare that they inflict on their prey, competitors, and predators [1]. The venom of the cone snail, which is injected through a disposable chitin-containing harpoon, consists of a diverse array of bioactive peptides which are typically 10–30 amino acids in length [2]. Structural rigidity appears to play a key role in the activity of these peptides. In particular, the conotoxins are a class of multiple disulfide-containing molecules that interact with nicotinic acetylcholine receptors (α-conotoxins), voltage-sensitive sodium channels (ω-conotoxins) and voltage-sensitive calcium channels (μ-conotoxins) [1]. The conantokins are Gla-containing peptides which have been shown to function as antagonists of the mammalian glutamate/glycine receptors of the *N*-methyl-D-aspartic acid (NMDA) subclass [3]. The NMDA receptor forms a cell-membrane ion channel that controls the flux of Ca^{2+} and Na^{+} into nerve cells. The receptor is activated only if Gly and Glu bind in concert and polyamines assist in the opening or closing of the ion channel, depending on their concentration. The action of conantokin-G (con-G) and presumably conantokin-T (con-T) has been attributed to the inhibition of the positive modulatory effects of polyamines [4]. When a stroke occurs, a detrimental influx of calcium initiates a cascade of events that eventually lead to neuronal cell death. Therefore, elucidating the mechanisms of NMDA antagonists and developing potent molecules to attenuate Ca^{2+} influx are the focus of intense research efforts.

Presumably, structural stabilization in the conantokin peptides is facilitated through calcium-chelation by the Gla residues [1,5]. In particular, apo-con-G was found to have very little helical content in aqueous solution, but it becomes almost completely helical (>85%) upon binding to calcium ions [5]. The conantokin-T peptide is also highly helical in the presence of calcium ions [1,3,5]. We recently investigated the calcium-binding properties of con-G (17-mer) and con-T (21-mer) by circular dichroism (CD) and potentiometry [6]. We proposed that divalent cation binding to con-T and con-G, chiefly to Gla residues contained in the peptides, is responsible for providing an active conformation that is able to interact with high affinity to its receptor site. Interestingly, at 25°C, apo-con-G has essentially no helical content (~0%) in aqueous solution but con-T exhibits a significant helical character (>40%) in the absence of divalent metal ions. We report here the solution structure of the conantokin-T peptide in the absence of divalent metal ions and under near neutral pH conditions. A detailed structure of apo-con-T will aid in the elucidation of the roles of metal binding in the biological activities of conantokin peptides. It also provides further evidence for the numerous interactions governing the conformational stability of helical peptides in the absence of disulfide bonds, metal ions or helix-inducing solvents [7].

2. Materials and methods

2.1. Sample preparation

The conantokin-T peptide was prepared by Fmoc chemistry on an Applied Biosystems (Foster City, CA) Model 433A Peptide Synthesizer and purified as described previously [6]. The peptide was dissolved in 10 mM sodium borate/100 mM NaCl to a final concentration of 2 mM. A volume of 50 μl of ^2H_2O was added to 450 μl of the peptide solution to provide the NMR deuterium lock signal. 4,4-Dimethyl-4-silapentane-1-sulfonate (DSS) was added as an internal reference. The pH of the sample was adjusted with dilute HCl to 6.5 to minimize the loss of NH signals at higher pH values. Lowering the pH value from our previous CD investigation (pH 8.0) had no significant effect on the molar residue ellipticity values at 222 nm.

*Corresponding author. Fax: (1) (514) 496-5143.
E-mail: feng.ni@nrc.ca

PII S0014-5793(97)00573-5

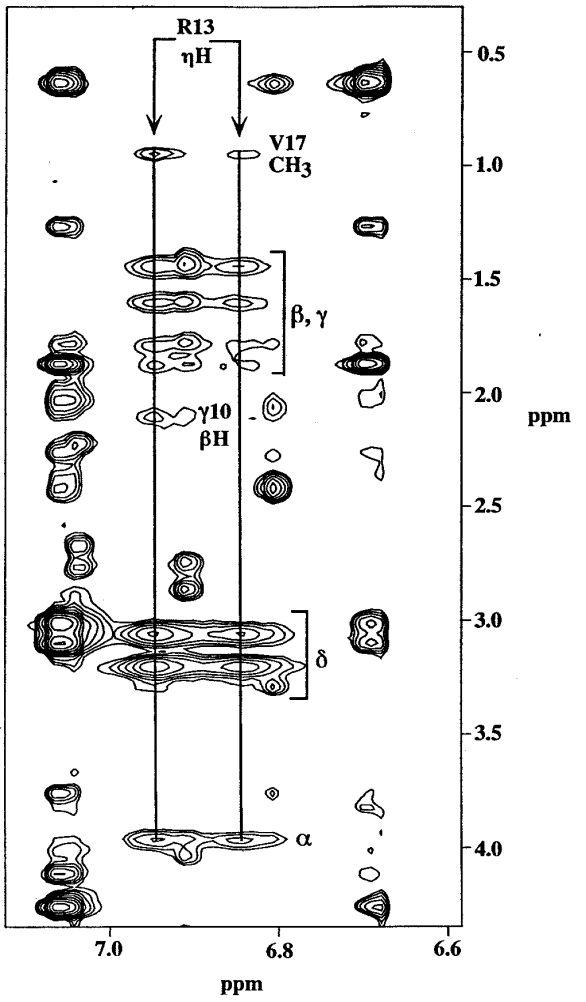

Fig. 1. Expanded view of the aromatic zone of a 250 ms NOESY spectrum of con-T at 5°C. Vertical lines dissect the NOE crosspeaks from the Arg^{13} guanidino protons, in addition to Val^{17} methyl protons and a βH of Gla^{10}.

2.2. NMR

One- and two-dimensional NMR experiments were carried out on a Bruker AMX2-500 and/or DRX-500 spectrometer using procedures as described previously [8,9]. TOCSY [10,11], flip-back NOESY [12] and DQF-COSY [13] spectra were acquired at 5, 15, and 25°C without spinning the sample. NOESY experiments were collected with mixing times of 150 and 250 ms. Spectral processing was carried out using FELIX (Hare Research) and an in-house program, nmrDSP, on Silicon Graphics workstations. Spectral contrast-enhancement methods were applied to resolve severely overlapped proton resonances [14,15]. The Sybyl software package (TRIPOS, Inc.) was used for spectral vizualization.

2.3. Proton resonance assignments

Sequence-specific assignments of the proton resonances for apo-con-T were achieved by combining the procedures of spin system identification using TOCSY, followed by sequential assignments through NOE connectivities [16]. The guanidino protons (H^{η}) of Arg^{13} were identified as a pair of moderately-broad signals in the NOESY spectra at 15°C and 5°C. Consistent with this assignment are the absence of TOCSY peaks but the presence of NOESY peaks, from the guanidino protons to all of the Arg^{13} side-chain and backbone protons. In particular, medium-strength NOEs are observed from the Arg^{13} guanidino protons to the εNH and δCH_2 protons (Fig. 1). In addition, the εNH of Arg^{13} exhibits an uncharacteristic downfield shift (7.72 ppm). All chemical shift values were determined from the 2D spectra and reported with respect to the DSS signal which was set to 0 ppm (Table 1).

2.4. Structure calculations

Peptide conformations free from steric overlaps and consistent with the NMR data were generated by distance geometry (DG) calculations utilizing the fixed bond lengths and bond angles provided in the ECEPP/3 database [17]. Optimization was achieved through a variable target function (VTF) implementation of distance geometry concepts, by varying all dihedral angles except for the ω angles governing the planarity of the peptide plane [18–20]. The set of backbone and side-chain dihedral angles were considered as independent variables during minimization of a distance target function or the ECEPP/3 potential energy [18,19]. Assigned NOE crosspeaks were characterized as strong, medium, or weak as determined from the number of contours and converted to distance upper bounds of 2.7, 3.7 and 5.0 Å, respectively. All side-chain to side-chain or side-chain to backbone medium range (i, i+2, i, i+3 and i, i+4) distance constraints were set to upper bounds of 5.0 Å, except for the $[d_{\alpha N}(i, i+3)]$ and $[d_{\alpha\beta}(i, i+3)]$ NOEs which were uniformly set to 3.7 Å (Table 2). The side chains of Asp, Glu, and Gla were treated as charged groups, Lys and Arg as neutral residues, and the hydrogen-bonding potentials of the Gln, Asn, Lys and Arg side-chains were eliminated during NOE distance-constrained energy minimization. In addition, charge interactions were screened by use of a sinusoidal distance-dependent dielectric function [20]. These empirical treatments of electrostatic interactions served to avoid potential bias of the computed NMR conformations by dominating electrostatic or hydrogen-bonding terms in the ECEPP force field. Further refinement of the peptide structures were carried out by distance-restrained Monte Carlo energy minimization [21]. Some overlapped NOEs were assigned based on the model structures generated from well-resolved NOE constraints. Remaining NOEs that could not be assigned uniquely were considered as ambiguous constraints that take into account all possible NOE interactions in an unbiased manner [19,20].

Table 1
Proton resonance assignments of conantokin-T at 5°C[a]

Residue	Chemical shift (ppm)			
	NH	αCH	βCH	Others
Gly^{1}		3.80, 3.94		
Glu^{2}	9.13	4.07	1.93*	γCH_2 2.21*
Gla^{3}	9.21	3.96	2.03*	γCH 3.06
Gla^{4}	8.07	3.89	2.21, 2.31	γCH 3.05
Tyr^{5}	8.11	4.21	2.96, 3.05	δCH_2 7.01; εCH2 6.65
Gln^{6}	8.16	3.71	2.00*	γCH_2 2.37*; εNH_2 8.01, 6.76
Lys^{7}	7.71	3.90	1.73*	γCH_2 1.38*; δCH_2 1.54*; εCH_2 2.81*; εNH_3 7.60
Met^{8}	7.75	3.99	2.30, 2.54	γCH_2 1.99, 2.22; εCH_3 1.82
Leu^{9}	7.88	3.77	1.22*	γCH_2 1.73; δCH_3 0.58*
Gla^{10}	8.09	3.95	2.05, 2.23	γCH 3.24
Asn^{11}	8.24	4.33	2.82, 2.69	δNH_2 7.60, 6.86
Leu^{12}	8.04	3.99	1.42*	γCH_2 1.69; δCH_3 0.73*
Arg^{13}	7.87	3.92	1.73, 1.83	γCH_2 1.40, 1.56; δCH_2 3.01, 3.15; εNH 7.72; ηH 6.90, 6.79
Gla^{14}	8.23	3.92	2.07, 2.13	γCH 3.14
Ala^{15}	7.99	4.00	1.36	
Glu^{16}	7.74	3.94	1.98*	γCH_2 2.17*
Val^{17}	7.81	3.61	2.08	γCH_3 0.80, 0.90
Lys^{18}	7.94	3.97	1.73*	γCH_2 1.35*; δCH_2 1.52*
Lys^{19}	7.92	3.95	1.71*	γCH_2 1.27*; δCH_2 1.46*
Asn^{20}	8.09	4.48	2.62, 2.72	δNH_2 7.57, 6.99
Ala^{21}	7.80	4.07	1.30	
Amide cap				7.28, 7.12

[a]These chemical shifts were determined at pH 6.5 with a peptide concentration of approximately 2 mM. The chemical shifts cited are relative to DSS which was set to 0 ppm. An asterix (*) indicates degenerate resonances.

Table 2
Distance input for structure determination

Sequential		
1 HA	2 HN	2.7, 2.0
2 HA	3 HN	3.7, 2.0
3 HA	4 HN	3.7, 2.0
4 HA	5 HN	3.7, 2.0
5 HA	6 HN	3.7, 2.0
6 HA	7 HN	3.7, 2.0
7 HA	8 HN	3.7, 2.0
9 HA	10 HN	3.7, 2.0
10 HA	11 HN	3.7, 2.0
11 HA	12 HN	3.7, 2.0
12 HA	13 HN	3.7, 2.0
16 HA	17 HN	3.7, 2.0
17 HA	18 HN	3.7, 2.0
20 HA	21 HN	3.7, 2.0
2 HN	3 HN	2.7, 2.0
3 HN	4 HN	2.7, 2.0
5 HN	6 HN	2.7, 2.0
6 HN	7 HN	2.7, 2.0
8 HN	9 HN	2.7, 2.0
9 HN	10 HN	3.7, 2.0
10 HN	11 HN	2.7, 2.0
11 HN	12 HN	2.7, 2.0
12 HN	13 HN	3.7, 2.0
13 HN	14 HN	2.7, 2.0
14 HN	15 HN	2.7, 2.0
15 HN	16 HN	3.7, 2.0
16 HN	17 HN	2.7, 2.0
17 HN	18 HN	3.7, 2.0
19 HN	20 HN	3.7, 2.0
20 HN	21 HN	3.7, 2.0
2 HB	3 HN	2.7, 2.0
4 HB	5 HN	3.7, 2.0
5 HB	6 HN	2.7, 2.0
6 HB	7 HN	3.7, 2.0
8 HB	9 HN	3.7, 2.0
9 HB	10 HN	3.7, 2.0
10 HB	11 HN	3.7, 2.0
11 HB	12 HN	3.7, 2.0
13 HB	14 HN	3.7, 2.0
14 HB	15 HN	3.7, 2.0
15 HM	16 HN	3.7, 2.0
17 HB	18 HN	3.7, 2.0
20 HB	21 HN	5.0, 2.0
Medium range: [backbone–backbone] and [backbone–side-chain]		
1 HA	3 HN	5.0, 2.0
2 HA	4 HN	5.0, 2.0
4 HA	6 HN	5.0, 2.0
5 HA	7 HN	5.0, 2.0
6 HA	8 HN	5.0, 2.0
9 HA	11 HN	5.0, 2.0
11 HA	13 HN	5.0, 2.0
17 HA	19 HN	5.0, 2.0
18 HA	20 HN	5.0, 2.0
2 HA	5 HN	3.7, 2.0
3 HA	6 HN	3.7, 2.0
5 HA	8 HN	3.7, 2.0
6 HA	9 HN	3.7, 2.0
8 HA	11 HN	3.7, 2.0
9 HA	12 HN	3.7, 2.0
11 HA	14 HN	3.7, 2.0
14 HA	17 HN	3.7, 2.0
15 HA	18 HN	3.7, 2.0
17 HA	20 HN	3.7, 2.0
2 HA	6 HN	5.0, 2.0
5 HA	9 HN	5.0, 2.0
11 HA	15 HN	5.0, 2.0
2 HN	4 HN	5.0, 2.0
3 HN	5 HN	5.0, 2.0
5 HN	7 HN	5.0, 2.0
13 HN	15 HN	5.0, 2.0

Table 2 (*continued*)

Medium range: [backbone–backbone] and [backbone–side-chain]		
14 HN	16 HN	5.0, 2.0
2 HA	5 HB	5.0, 2.0
5 HA	8 HB	5.0, 2.0
6 HA	9 HB	5.0, 2.0
8 HA	11 HB	5.0, 2.0
9 HA	12 HB	5.0, 2.0
11 HA	14 HB	5.0, 2.0
14 HA	17 HB	5.0, 2.0
17 HA	20 HB	5.0, 2.0
Intraresidue and [side-chain–side-chain]		
1 HA	2 HB	5.0, 2.0
2 HA	5 HD	5.0, 2.0
3 HA	5 HD	5.0, 2.0
5 HD	8 HN	5.0, 2.0
5 HD	7 HN	5.0, 2.0
5 HD	9 HB	5.0, 2.0
5 HD	9 HM	5.0, 2.0
5 HD	8 HM	5.0, 2.0
5 HD	8 HG	5.0, 2.0
5 HD	8 HB	5.0, 2.0
5 HD	5 HB	5.0, 2.0
5 HD	6 HA	5.0, 2.0
5 HD	5 HA	5.0, 2.0
5 HD	9 HN	5.0, 2.0
5 HE	9 HM	5.0, 2.0
5 HE	9 HB	5.0, 2.0
5 HE	8 HM	3.7, 2.0
5 HE	5 HB	5.0, 2.0
5 HE	6 HA	5.0, 2.0
5 HD	6 HG	5.0, 2.0
5 HE	9 HN	5.0, 2.0
5 HD	6 HN	5.0, 2.0
5 HE	6 HN	5.0, 2.0
5 HD	5 HN	5.0, 2.0
6 HA	9 HM	5.0, 2.0
6 HG	10 HG	5.0, 2.0
6 HB	9 HM	5.0, 2.0
6 HB	9 HB	5.0, 2.0
6 HN	6 HB	5.0, 2.0
6 HN	6 HG	5.0, 2.0
6 HN	7 HB	5.0, 2.0
6 HN	9 HB	5.0, 2.0
6 HN	9 HM	5.0, 2.0
6 HE1	9 HM	5.0, 2.0
6 HE2	9 HM	5.0, 2.0
6 HE2	10 HG	3.7, 2.0
6 HE1	10 HG	3.7, 2.0
6 HE1	5 HD	5.0, 2.0
6 HE1	5 HE	5.0, 2.0
7 HE	7 HN	5.0, 2.0
8 HB	8 HM	5.0, 2.0
8 HG	9 HB	5.0, 2.0
8 HA	11 HD	3.7, 2.0
8 HM	12 HM	3.7, 2.0
8 HM	9 HM	5.0, 2.0
8 HM	9 HB	3.7, 2.0
8 HG	12 HM	5.0, 2.0
8 HB	8 HG	5.0, 2.0
8 HG	9 HB	5.0, 2.0
8 HG	9 HN	5.0, 2.0
8 HB	8 HN	5.0, 2.0
8 HG	11 HB	5.0, 2.0
9 HA	12 HM	5.0, 2.0
9 HA	12 HG	5.0, 2.0
9 HB	10 HG	5.0, 2.0
9 HM	12 HB	5.0, 2.0
9 HM	10 HN	3.7, 2.0
9 HG	10 HN	5.0, 2.0
10 HG	11 HN	5.0, 2.0
10 HB	11 HB	5.0, 2.0

Table 2 (*continued*)

Intraresidue and [side-chain–side-chain]		
11 HN	12 HM	5.0, 2.0
11 HB	12 HM	5.0, 2.0
11 HD	11 HB	5.0, 2.0
11 HD	11 HA	5.0, 2.0
11 HD	11 HN	5.0, 2.0
12 HM	16 HG	5.0, 2.0
12 HM	13 HB	5.0, 2.0
12 HM	15 HM	5.0, 2.0
12 HM	11 HN	5.0, 2.0
13 Hη	17 HM1	5.0, 2.0
13 HB	10 HN	5.0, 2.0
13 HD	13 HN	5.0, 2.0
13 HG	17 HM	5.0, 2.0
13 HB	14 HN	5.0, 2.0
13 HG	14 HN	5.0, 2.0
13 HD	14 HN	5.0, 2.0
14 HG	17 HM1	5.0, 2.0
14 HG	17 HN	5.0, 2.0
14 HG	18 HN	5.0, 2.0
14 HA	17 HM	5.0, 2.0
14 HG	15 HN	3.7, 2.0
14 HB	15 HN	3.7, 2.0
15 HN	17 HM	5.0, 2.0
16 HG	17 HM	5.0, 2.0
17 HM1	21 HM2	5.0, 2.0
20 HD	16 HB	5.0, 2.0
20 HD	17 HA	5.0, 2.0
21 NHt	19 HA	5.0, 2.0
21 NHt	20 HA	5.0, 2.0
Group NOEs		
X5	X1	5.0, 2.0
X5	X2	5.0, 2.0
X5	X3	5.0, 2.0
X6	X1	5.0, 2.0
X7	X1	5.0, 2.0
X8	X4	5.0, 2.0
X10	X11	5.0, 2.0
X9	X14	5.0, 2.0
X10	X13	5.0, 2.0
X5	X1	5.0, 2.0
X16	X15	5.0, 2.0
X17	X18	5.0, 2.0
X19	X20	5.0, 2.0
X19	X21	5.0, 2.0
X19	X22	5.0, 2.0
X17	X26	5.0, 2.0
X8	X27	5.0, 2.0

Table 2 (*continued*)

Group definitions		
X1	7 HB,	13 HB
X2	7 HG,	13 HG
X3	7 HD,	13 HD
X4	13 HB	
X5	11 HD	
X6	10 HG	
X7	11 HB2	
X8	16 HB,	17 HB
X9	6 HG	
X10	4 HG,	5 HB
X11	13 HE,	7 HN
X12	10 HG	
X13	2 HG,	4 HB
X14	7 HB,	9 HG
X15	15 HM,	18 HG
X16	16 HB	
X17	17 HM1	
X18	13 HA,	14 HA
X19	14 HG	
X20	13 HB,	18 HB
X21	13 HD,	18 HD
X22	13 HG,	18 HG
X23	11 HB	
X24	14 HB1,	10 HB1
X25	16 HG	
X26	18 HG,	15 HM
X27	18 HB,	19 HB

3. Results and discussion

3.1. Conantokin-T has a high helical content in the absence of metal binding

Previous investigations demonstrated that apo-con-T is significantly helical in aqueous solution and at 25°C [5,6]. Lowering the temperature to 5°C resulted in an increase of helical content to approximately 55%, as determined by CD. This value is an under estimation of the true helical content as the result of a contribution by tyrosine to the CD signal at 222 nm [22]. The proton resonance linewidths and chemical shifts remained constant over approximately 0.5 to 4.0 mM, suggesting that the peptide remains monomeric in aqueous solution at the concentration (2 mM) used for NMR analysis. This result is consistent with our previous studies using CD and gel permeation chromatography [6], indicating that structure formation with apo-con-T is an intrinsic property of the monomeric peptide. The significant helical content of this peptide may be rationalized by an inspection of the primary sequence of the con-T peptide (Fig. 2). Reminiscent of a de novo designed alanine-based peptide, each charged residue has at least one oppositely charged side-chain to interact with at positions (*i*, *i*+3 or *i*, *i*+4) that are favored in helical conformations [23]. Likewise, the majority of the hydrophobic residues are also appropriately spaced, such that stabilizing contacts may be formed [7,24]. The presence of negatively charged residues at the N-terminus (Glu^2-Gla^3-Gla^4) and positively charged amino acids at the C-terminus (Lys^{18}-Lys^{19}) could provide stabilization of the helix macro-dipole. The potential to form many of the known helix-stabilizing interactions therefore exist in this peptide and extend from the N- to C-termini.

Conformations of apo-con-T can be examined on a residue-specific basis by use of NMR after the assignment of all the proton resonances. The chemical shifts of the H^α protons are generally dependent on molecular conformation, composition and environment. But after subtracting the values estimated for a random-coil state, the resulting differences (or conformational shifts) are strongly related to the backbone conformation or the secondary structure, independent of the sequence of the peptide [25,26]. Upfield shifts of 0.1 ppm or greater for the H^α resonances, when compared to the random-coil values, are indicative of a helical structure, if this occurs over four or more adjacent residues. Fig. 3 shows the conformational shifts of the H^α proton resonances for every residue of the con-T peptide. The random-coil value of 4.18 ppm for the Gla residue was determined from the NMR spectra of con-T in the presence of 6 M urea. A larger than 0.2 ppm upfield shift for all the H^α protons indicates that apo-con-T assumes a well-folded helical structure from Glu^2 all the way to Ala^{21}, the end of the peptide. In addition, con-T has strong sequential

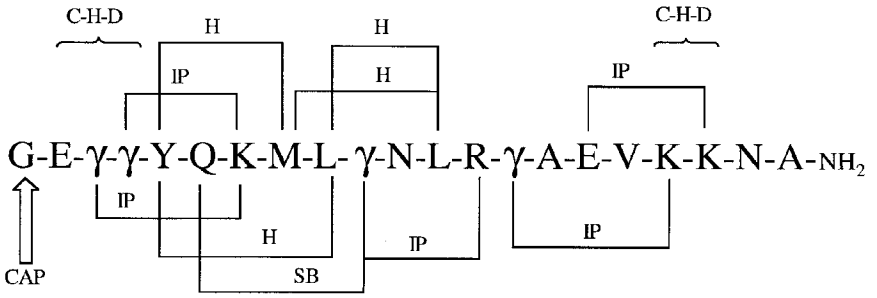

Fig. 2. The amino acid sequence of the conantokin-T peptide. Potential side-chain interactions are indicated on the solid line connecting each pair of residues. The following abbreviations are used: IP, ion pair; SB, salt-bridge; H, hydrophobic interaction; CAP, favorable capping residue; CHD, favorable charge-helix-dipole interaction.

backbone NH-NH NOEs [$d_{NN}(i, i+1)$] and exhibits many characteristic medium-range backbone-backbone [$d_{\alpha N}(i, i+3)$] and backbone-side-chain [$d_{\alpha\beta}(i, i+3)$] NOE contacts throughout the peptide (Fig. 4). Most of these NOEs also exist in the NOESY spectra acquired at higher temperatures, as long as the involved protons have well-resolved resonances. The majority of [$d_{\alpha N}(i, i+1)$] NOEs (Fig. 5) were found to be significantly weaker than the corresponding [$d_{NN}(i, i+1)$] crosspeaks, consistent with a high degree of helical structure. Furthermore, three-bond coupling constants, $J_{\alpha N}$, between the H^{α} and the NH protons are around 5 Hz for residues with well-resolved H^{α}-NH correlation peaks (e.g., residues Gla^{3}, Lys^{7}, Asn^{11}, and Val^{17}) and the backbone NH protons showed very small temperature-induced upfield shifts of less than 4 ppm/K and even increased (downfield-shifted) chemical shifts for some residues (data not shown). All these NMR parameters indicate that apo conantokin-T is almost entirely helical in aqueous solution with very little population of additional conformations. In addition, the peptide may be strongly α-helical since the intensities of the [$d_{\alpha N}(i, i+2)$] NOEs (Fig. 4) are comparable with those of the [$d_{\alpha N}(i, i+4)$] NOEs and are much weaker than those of the [$d_{\alpha N}(i, i+3)$] NOEs.

3.2. Apo-con-T has extensive side-chain NOE contacts

In addition to the multitude of backbone NOEs, there are also many NOE connectivities (Table 2) between the side-chain protons of the potential contact residues in a helical conformation (Fig. 2). For example, the aromatic ring protons of Tyr^{5} exhibit strong NOEs to both the methyl protons of residues Met^{8} and Leu^{9}. In addition, the methyl protons of residues Met^{8} and Leu^{9} have NOE interactions with the methyl protons of Leu^{12}. These side-chain NOEs indicate that there must be a well-defined hydrophobic cluster between residues Tyr^{5}, Leu^{9}, Met^{8}, and Leu^{12} for apo-conantokin-T in solution. This hydrophobic cluster remains over the temperature range of 5–25°C since almost all of the NOEs are still observed in the respective NOESY spectra (not shown). More strikingly, the side-chain NOEs between residues Tyr^{5}, Leu^{9}, Met^{8}, and Leu^{12} persist in the presence of 6 M urea, indicating that the four hydrophobic residues remain in contact even under unfolding conditions.

Apart from NOEs among the side chains of hydrophobic residues, the guanidino protons of Arg^{13} (at 6.90 and 6.79 ppm, Table 1) also make NOE contacts to a methyl group of residue Val^{17} and to a βH proton of Gla^{10} (Fig. 1). The same Val^{17} methyl group displays an NOE connectivity to the γ-proton of Gla^{14} (Table 2). There are also various Arg^{13}/Gla^{14} side-chain NOE contacts. Contacts involving the side-chain amide protons have also been characterized for the conantokin-T peptide. In particular, the side-chain amide protons of Gln^{6} are adjacent to the γ-hydrogen of Gla^{10} and to the methyl groups of Leu^{9}. The Asn^{20} side-chain amide interacts with the backbone, as indicated by an NOE contact with the H^{α} proton of Val^{17}. The terminal amide proton is in spatial proximity to the alpha hydrogens of Lys^{19} and Asn^{20}. The observation of relatively sharp Arg^{13} guanidino protons are especially noteworthy because they are usually very broad as a result of rapid exchange with solvent water protons [27]. In addition, the presence of NOEs to the side chain of Arg^{13} indicates that interactions involving this residue may be very significant in the conantokin-T peptide.

3.3. The α-helical structure of apo-conantokin T in solution

The structure of apo-con-T was generated from a total of 167 distance constraints (Table 2) derived from 12 intraresidue, 70 sequential and 85 medium-range (*i*, *i*+2, *i*, *i*+3, and *i*, *i*+4) NOEs. Initially five-hundred structures were generated by distance geometry calculations. Fig. 6 shows a cluster of 10 converged structures after Monte Carlo energy minimization with RMSD values of 0.40 and 0.77 Å for the backbone and all the heavy atoms, respectively. Clearly, the backbone of

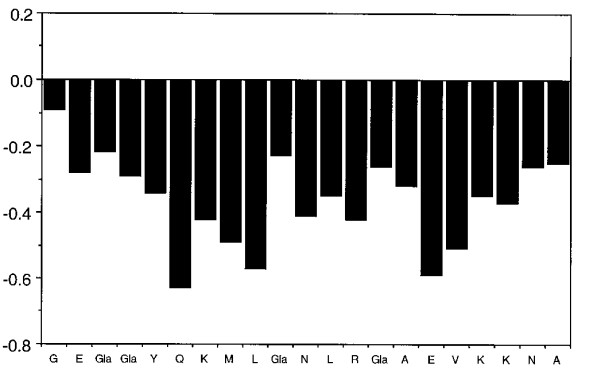

Fig. 3. Chemical shift index for the H^{α}-proton resonances of con-T in 90% aqueous (10 mM sodium borate/100 mM NaCl)/10% D_2O, pH 6.5, at 5°C. The values for each residue were calculated through subtraction of the corresponding random coil chemical shift value (Wishart et al, 1995) from the measured value. The random coil value for the Gla residue was estimated as 4.18 ppm (see the text).

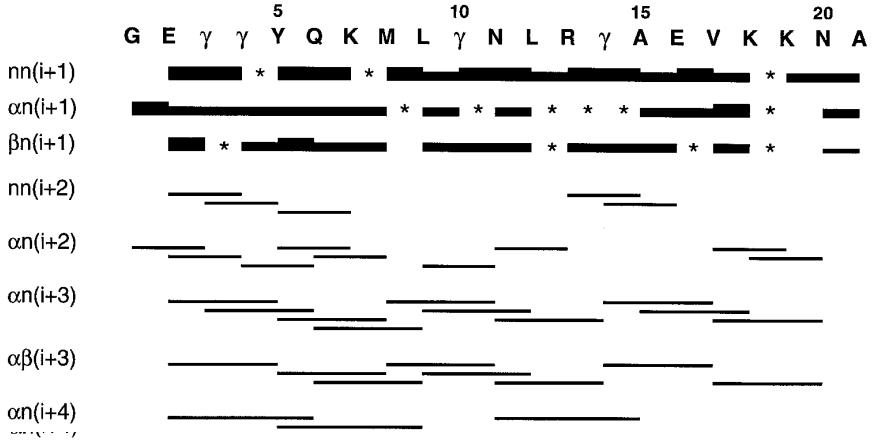

Fig. 4. Summary of the sequential and interresidue NOEs observed for con-T at 5°C, pH 6.5. An asterix indicates that the assignment of an observed cross peak was ambiguous due to resonance overlaps. The height of the bar provides a qualitative measure of the intensities of the NOEs in the NOESY (150 or 250 ms mixing time) spectrum of con-T. Included in this figure are a few medium-range NOEs that are degenerate or partially overlapped at 5°C, but that were resolved and verified at higher temperatures.

apo-con-T is a particularly well-defined α-helix with almost no fraying at both the N- and C-terminal ends of the helix. The well-folded α-helical conformation of apo-conantokin-T is therefore in contrast to the structures of other monomeric helices where end fraying was still observed even with optimized capping interactions [7,28]. The conantokin-T helix also has well-defined side-chain conformations (Fig. 6), apparently owing to the presence of many side-chain NOE interactions (Table 2).

The three-dimensional structure of apo-conantokin-T has a unique character with the hydrophobic side chains of Tyr^5, Met^8, Leu^9, and Leu^{12} grouped together on one face of the molecule together with the side chain of Glu^2 and the Glu^{16}-Lys^{19} ion-pair (Fig. 6). The opposite face is highly charged

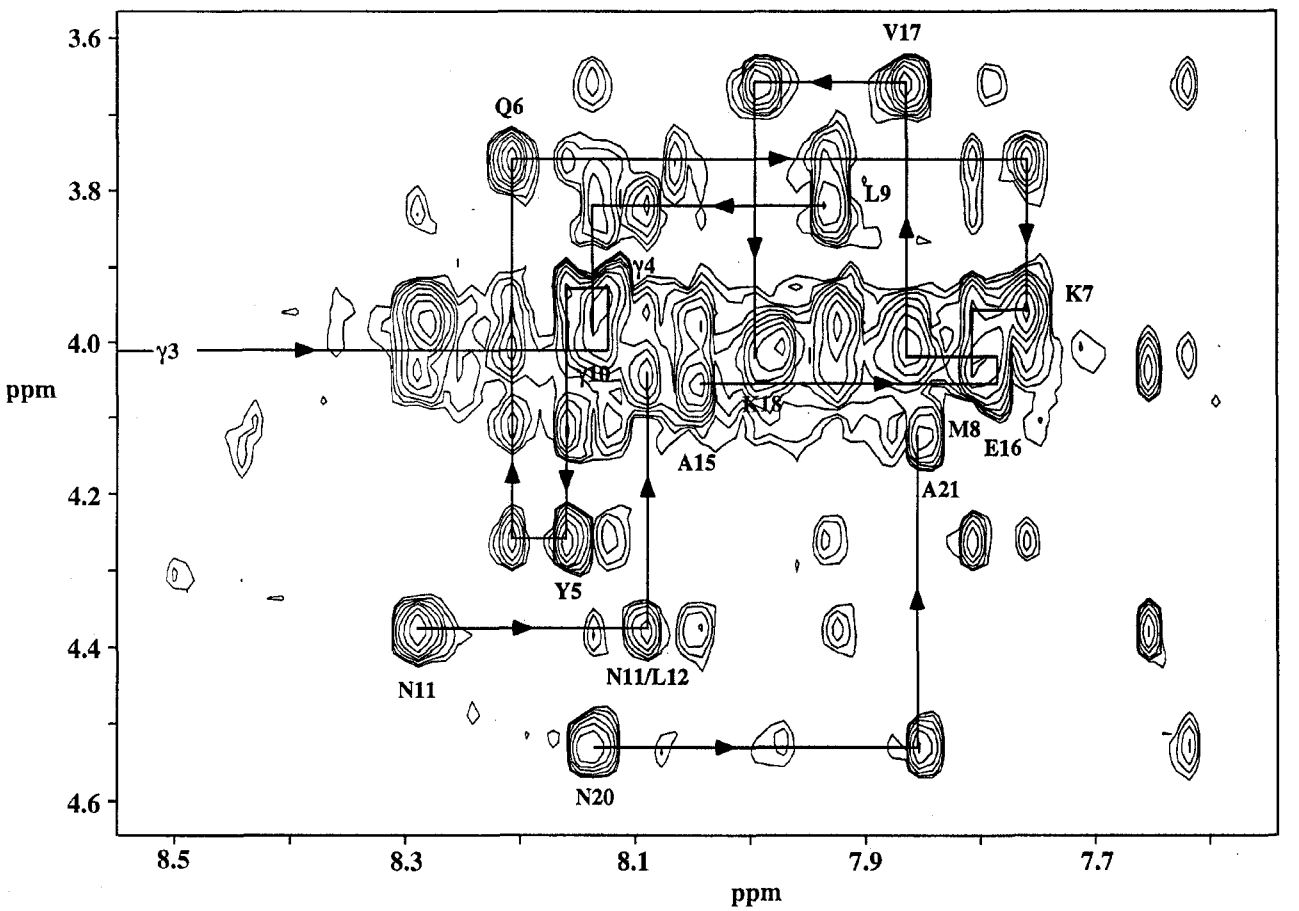

Fig. 5. NH-H^{α} region of a 250 ms mixing time NOESY spectrum of con-T in 90% aqueous (10 mM sodium borate/100 mM NaCl)/10% ^2H_2O, pH 6.5, at 5°C. Glu^2 and Gla^3 are shifted downfield at 9.13 and 9.21 ppm, respectively.

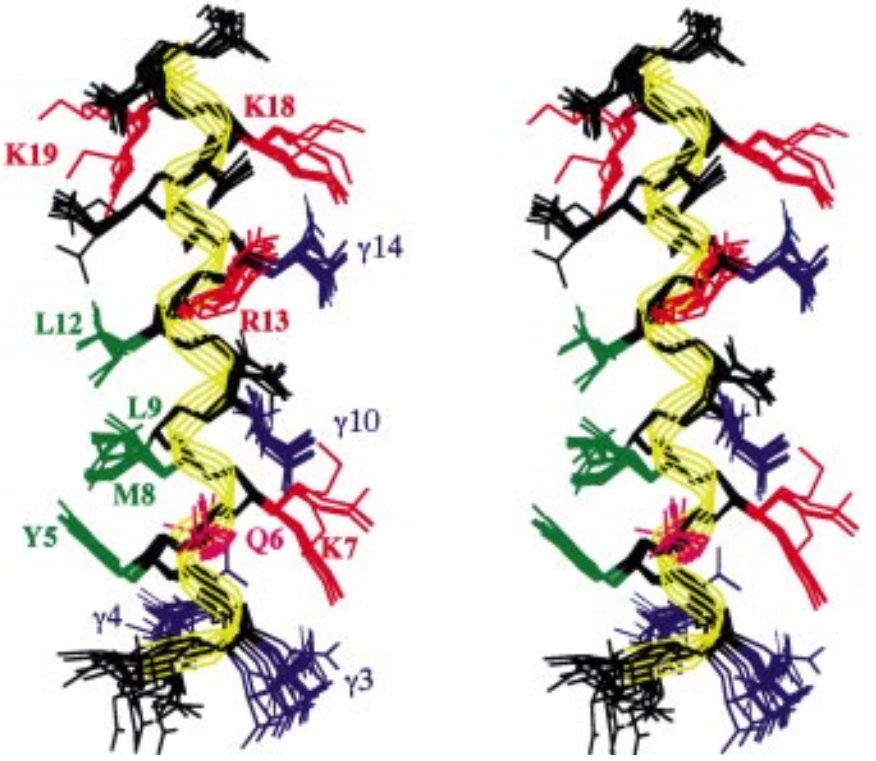

Fig. 6. A stereoview of a cluster of 10 low energy conformations of con-T derived from distance geometry calculations followed by Monte Carlo energy minimization. The structures were superimposed using the C^{α} atoms of all the residues (Gly^{1}-Ala^{21}). Positively charged side-chains (Lys^{7}, Arg^{13}, Lys^{18}, and Lys^{19}) are colored in red, the Gla residues (Gla^{3}, Gla^{4}, Gla^{10} and Gla^{14}) are in blue, Gln^{6} is magenta, and the hydrophobic cluster (Tyr^{5}, Met^{8}, Leu^{9} and Leu^{12}) is shown in green. The backbone conformations of all the structures are in the α-helical region ($\phi \sim -60$, $\psi \sim -40$) for all residues from Gla^{3} to Ala^{21}. The well-defined structure of the apo-con-T α-helix is a direct consequence of the many NOE contacts among the amino acid side chains (Table 2), in addition to the backbone NOE connectivities (Fig. 4).

and consists of a potential Gla^{3}-Lys^{7} ion pair, a Gla^{10}-Arg^{13}-Gla^{14}-Lys^{18} electrostatic network and a Gln^{6}-Gla^{10} hydrogen bonding contact. The interaction between Gla^{10} and Arg^{13} is mediated in addition by a hydrogen bond between one of the carboxylate groups of Gla^{10} and the εNH proton of Arg^{13}, presumably responsible for an downfield shifted NH proton resonance for the Arg^{13} side chain (Table 1). These electrostatic interactions and hydrogen bonding contacts are the direct consequence of the NOE distance constraints since Arg and Lys were treated as neutral and the hydrogen-bonding potential of the Gln, Asn, Arg and Lys side chains was eliminated during the calculation of the structures (see the Section 2).

At the beginning of the helix, the positively-charged free N-terminus appears to be in contact with the negatively-charged side chain of Gla^{4} (Fig. 6). The three exposed backbone NH groups of residues Glu^{2}, Gla^{3} and Gla^{4} seem to have strong interactions with one of the carboxylate groups of Gla^{4}, making Gla^{4} the apparent capping residue with side-chain to main-chain hydrogen bonding interactions. In all, the negatively charged side chains of residues Glu^{2}, Gla^{3} and Gla^{4} face away from one another, apparently to minimize electrostatic repulsion among the five negative charges (Glu^{2}, −1; Gla^{3}, and Gla^{4}, −2). On the C-terminal end of the helix, the exposed carbonyl groups appear to be capped by the side-chain amides of Asn^{20} and by the amide group of the last residue Ala^{21}, which presumably minimizes the fraying of the helix through hydrogen bonding interactions.

Within the hydrophobic cluster, Tyr^{5} and Leu^{12} appear not to be in direct contact but are positioned on opposite sides of the Met^{8}/Leu^{9} interaction. The large non-polar surface area of Tyr^{5} seems to accommodate both a sulfur-containing side chain of residue Met^{8}, as well as the aliphatic side chain of residue Leu^{9}. Although quantitation of these interactions was not yet attempted, stabilization of the helical conformation by these hydrophobic residues must be significant since the hydrophobic contacts persist even in the presence of 6 M urea. The arrangement of the polar side chains in conantokin-T is particularly interesting: residues Gla^{10} and Gla^{14} are immersed in between residues Gln^{6}, Arg^{13} and Lys^{18} in the following array of electrostatic/hydrogen-bonding interactions: Gln^{6}-Gla^{10} followed by Gla^{10}-Arg^{13} followed by Arg^{13}-Gla^{14} and followed by Gla^{14}-Lys^{18} (Fig. 6). The Gln^{6}-Gla^{10} and Arg^{13}-Gla^{14} interactions appear to be particularly strong with close spatial proximities while residue Arg^{13} in addition serves to link the two pairs together. In addition to potential charge-helix dipole interactions, both the negatively charged Glu^{2}, Gla^{3} and Gla^{4} and the positively-charged Lys^{18} and Lys^{19} serve specific structure roles in the maintenance of the helical conformation of the apo peptide in solution.

3.4. Implications for the biological activities of conantokin peptides

No clear relationship has yet been established between the degree of helicity and the binding potency in terms of the biological functions of the con-G/con-T peptides [1,3,5,29,30]. Regardless, our studies demonstrated that the α-helical conformation is an intrinsic property of the conan-

tokin-T peptide independent of the binding of metal ions. The well-folded nature of the apo-con-T helix (Fig. 6) also implies the importance of the helical structure for the biological activities, since binding-induced unfolding of an α-helix with many stabilizing interactions (Fig. 6) would be energetically unfavorable and at the expense of a tremendously reduced binding affinity. Assuming a helical structure for the bioactive conformation, the precise spatial dispositions of the amino acid side chains would be more important than those of the peptide backbone for binding interactions with the receptor. A receptor-bound helical structure of the conantokin peptides such as that shown in Fig. 6 also accounts for the observation that the binding potency is strongly dependent on the types of amino acid side chains in a few locations of the peptide sequence [29,30]. The binding of divalent metal ions to con-T presumably induces conformational changes in the side chains of the amino acids required for optimal interactions with the receptor protein. Indeed, preliminary NMR results indicate that calcium binding to the con-T peptide results in significant changes only in the orientations of a few side chains with well-defined helical conformations for all amino acid residues (unpublished observations).

In summary, the presence of many helix stabilizing interactions in apo-conantokin-T confers its ability to exist as a highly structured molecule in aqueous solution. The solution structure of apo-con-T is essential for characterizing the conformational changes induced by metal binding and for developing a more detailed understanding of conantokin peptide structure-function relationships. This study also provided further evidence for hydrophobic, electrostatic and hydrogen-bonding interactions that stabilize an isolated α-helix in solution. Similar conclusions have been reached on the basis of the solution conformations of con-G and con-T reported in a recent study independent of this work [31]. Our results indicate that apo-con-T has a well-defined α-helical structure even to the positions of many amino acid side chains (Fig. 6). Therefore, there may be less changes in the conformation of the conantokin-T peptide upon the binding of divalent metal ions as one may infer from a mixture of α- and 3_{10}-helices with distorted backbone conformations determined for apo-con-T in the previous NMR study [31].

Acknowledgements: We thank Dr. Daniel Ripoll of the Cornell University Theory Center for providing the coordinates and force fields for the charged Gla residue. This work was supported by grant HL-19982 from the National Institutes of Health, the Kleiderer-Pezold family endowed professorship (to F.J.C.), grants from the Medical Research Council of Canada (MT-12566) and from Ciba-Geigy Canada Ltd. (to F.N.), a postdoctoral fellowship from the American Heart Association, Indiana Affiliate (to M.P.), a predoctoral fellowship from the American Heart Association, Indiana Affiliate (to S.E.W.) and by the National Research Council of Canada (NRCC publication No. 39968).

References

[1] Myers, R.A., Cruz, L.J., Rivier, J.E. and Olivera, B.M. (1993) Chem. Rev. 93, 1923–1936.
[2] Olivera, B.M., Gray, W.R., Zeikus, R., McIntosh, J.M., Varga, J., de Santos, V. and Cruz, L.J. (1985) Science 230, 1338.
[3] Haack, J., Rivier, J., Parks, T., Mena, E., Cruz, L. and Oliver, B.M. (1990) J. Biol. Chem. 265, 6025–6029.
[4] Skolnick, P., Boje, K., Miller, R., Pennington, M. and Maccecchini, M.-L. (1992) J. Neurochem. 59, 1516–1521.
[5] Myers, R.A., McIntosh, J.M., Imperial, J., Williams, R.W., Oas, T., Haack, J.A., Hernandez, F., Rivier, J., Cruz, L.J. and Olivera, B.M. (1990) J. Toxicol.-Toxin Reviews 9, 179–202.
[6] Prorok, M., Warder, S.E., Blandl, T. and Castellino, F.J. (1996) Biochemistry 35, 16528–16534.
[7] Muñoz, V. and Serrano, L. (1995) Curr. Opin. Biotech. 6, 382–386.
[8] Ni, F., Ripoll, D.R., Martin, P.D. and Edwards, B.F.P. (1992) Biochemistry 31, 11551.
[9] Ni, F. (1992) J. Magn. Reson. 99, 391–397.
[10] Braunschweiler, L. and Ernst, R.R. (1983) J. Magn. Reson. 53, 521–528.
[11] Davis, D.G. and Bax, A. (1985) J. Am. Chem. Soc. 107, 2820–2821.
[12] Lippens, G., Dhalluin, C. and Wieruszeski, J.-M. (1995) J. Biomol. NMR 5, 327–331.
[13] Rance, M., Sorenson, O.W., Bodenhausen, G., Wagner, G., Ernst, R.R. and Wüthrich, K. (1983) Biochem. Biophys. Res. Commun. 117, 479–495.
[14] Zhu, Y. (1992) An Iterative Algorithm for 2D NMR Spectral Enhancement Technical Report, Department of Electrical Engineering, Syracuse University.
[15] Levy, G.C., Jeong, G.N.and Zhu, Y. (1992) Maximum-Likelihood Spectral Deconvolution and its Utilization in Quantitative Multidimensional NMR. p. 152, Proceedings of the 33rd Exp. NMR Conference.
[16] Wüthrich, K. (1986) NMR of Proteins and Nucleic Acids, John Wiley and Sons, Inc., New York.
[17] Némethy, G., Gibson, K.D., Palmer, K.A., Yoon, C.N., Paterlini, G., Zagari, A., Rumsey, S. and Schereaga, H.A. (1992) J. Phys. Chem. 96, 6472–6484.
[18] Vásquez, M. and Scheraga, H.A. (1988) J Biomol. Struct. Dyn. 5, 757–784.
[19] Ni, F., Konishi, Y. and Scheraga, H.A. (1989) Biochemistry 29, 4479–4489.
[20] Ni, F., Zhu, Y. and Scheraga, H.A. (1995) J. Mol. Biol. 252, 656–671.
[21] Ripoll, D.R. and Ni, F. (1992) Biopolymers 32, 359–365.
[22] Chakrabartty, A., Kortemme, T., Padmanabhan, S. and Baldwin, R.L. (1993) Biochemistry 32, 5560–5565.
[23] Scholtz, J.M., Qian, H., Robbins, V.H. and Baldwin, R.L. (1993) Biochemistry 32, 9668–9676.
[24] Scholtz, J.M. and Baldwin, R.L. (1992) Annu. Rev. Biophys. Biomol. Struct. 21, 95–118.
[25] Wishart, D.S., Sykes, B.D. and Richards, F.M. (1992) Biochemistry 31, 1647–1651.
[26] Wishart, D.S., Bigam, C.G., Holm, A., Hodges, R.S. and Sykes, B.D. (1995) J. Biomol. NMR 5, 67–81.
[27] Yamazaki, T., Pascal, S.M., Singer, A.U., Formann-Kay, J.D. and Kay, L.E. (1995) J. Am Chem Soc. 117, 3556–3564.
[28] Gong, Y.X., Zhou, H.X., Gou, M.M. and Kallenbach, N.R. (1995) Protein Sci. 4, 1446–1456.
[29] Chandler, P., Pennington, M., Maccecchini, M.L., Nashed, N.T. and Skolnick, P. (1993) J. Biol. Chem. 268, 17173–17178.
[30] Zhou, L.-M., Szendrei, G.I., Fossom, L.H., Maccecchini, M.L., Skolnick, P. and Otvos Jr., L. (1996) J. Neurochem. 66, 620–628.
[31] Skjaerbaek, N., Nielsen, K.J., Lewis, R.J., Alewood, P. and Craik, D.J. (1997) J. Biol. Chem. 272, 2291–2299.